

# Giant subthreshold amplification in synchronously pumped optical parametric oscillators

G. D'Alessandro<sup>1</sup> and F. Papoff<sup>2</sup><sup>1</sup>*School of Mathematics, University of Southampton, Southampton SO17 1BJ, United Kingdom*<sup>2</sup>*Department of Physics, SUPA, University of Strathclyde, Glasgow G4 0NG, United Kingdom*

(Received 7 May 2009; published 7 August 2009)

Synchronously pumped parametric oscillators have been shown to have subthreshold giant amplification of such a magnitude that a macroscopic, entirely noise-driven, signal is present at output even when the device is below threshold. In this paper we quantify the magnitude of the amplification factor in terms of some key device parameters. We use non-normal operator theory to find the noise amplification factor (Kreiss constant) and show that the signal amplitude is proportional to it. We also determine that the noise sensitivity depends in a nontrivial way on the group velocity of the three fields.

DOI: [10.1103/PhysRevA.80.023804](https://doi.org/10.1103/PhysRevA.80.023804)

PACS number(s): 42.65.Yj

## I. INTRODUCTION

Noise in physical systems is often treated as a small perturbation, a weak interaction with the environment that is responsible, for example, for moving the system away from unstable equilibria. Generally, noise is considered relatively insignificant near a stable equilibrium. This point of view, while often correct, has notable exceptions. One of the most famous is stochastic resonance [1], where noise can enhance the response of a system to small external forcing. Another is giant noise amplification, also called *excess noise*. In optics, for example, excess noise [2,3] is normally associated to cavities with nonorthogonal modes. However, it has been known for quite some time that the phenomenon is more general [4,5] and is state dependent [6]. The most famous example of giant noise amplification is the development of turbulence from laminar flows [7]: linear stability analysis of some laminar flows predicts instability thresholds that are much higher than those observed experimentally. The explanation of this inconsistency proposed in [7] is that these flows are extremely sensitive to noise: small amplitude noise is amplified enormously by the subthreshold dynamics so that it becomes macroscopically observable even though the laminar flow is stable. The mathematical equivalent of this physical interpretation is that the linear stability operator of these noise-sensitive flows is highly non-normal, i.e., has eigenvectors that are nearly parallel (see the Appendix and Refs. [7,8]). The theory of non-normal operators has led in the mathematical and numerical analysis literature to the development of tools to characterize and quantify the response of (stable) systems to perturbations, namely, the pseudospectrum (see [9] for a historical overview of the field and [10] for a list of references to pseudospectra, non-normal operators and their applications). At the same time, noise-sensitive systems have also been studied in the physics literature outside optics. For example, a recent paper [11] studies noise sensitivity in a Bose-Einstein condensate in an optical resonator, but still in the context of excess noise. The non-normal operator approach seems, to the best of our knowledge, to be mainly focused in physics areas related to numerical analysis [12] or fluid dynamics [13–15].

In this paper, we use the tools of non-normal operators and pseudospectra to analyze in detail a model of synchronously pumped optical parametric oscillators (SPOPOs). These are physical systems of great importance in nonlinear

optics that show giant noise amplification. SPOPOs contain a nonlinear  $\chi^{(2)}$  crystal, i.e., a crystal with quadratic nonlinearity as, for example, lithium niobate, that can transform an input beam at frequency  $\omega_1$ , the pump, in two output beams, the signal and the idler, at frequency  $\omega_2$  and  $\omega_3$ , respectively. The crystal is placed in an optical cavity (see Fig. 1) so that one or more of the fields are resonated. In the case considered in this paper only the signal beam is resonated: the mirrors are transparent to the pump and idler. The device is driven by a train of pump pulses with period  $T_R$ , very close to the cavity round trip time of the signal pulses,  $T_c$ . In this configuration, the SPOPO can be used as a tunable source of laser pulses: in particular, the signal pulses may be considerably shorter than the pump pulses [16–20]. This regime was analyzed in some detail in [21], where it was shown that the signal pulses have chaotic dynamics that is extremely noise sensitive: they change from one round trip to the next and never settle in an equilibrium configuration. The issue of sensitivity to noise was taken up again in [22] where it was shown, using pseudospectra and the theory of non-normal operators, that a *subthreshold* SPOPO can amplify noise fluctuation by a factor of  $10^9$ : this factor is so large that a macroscopic, entirely noise driven signal field is emitted by the device, even though it is subthreshold, i.e., even though the zero-signal field solution is stable.

This phenomenon is considerably different from nonresonant optical parametric amplification because the presence of the cavity introduces feedback in the system. This, by itself, is unable to sustain a non-zero-signal field. However, in the

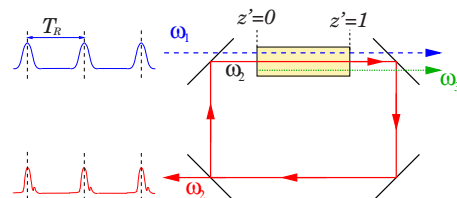


FIG. 1. (Color online) Schematic of a SPOPO. The shaded rectangle represents a  $\chi^{(2)}$  material. The pump field, at frequency  $\omega_1$ , is seeded by a periodic train of pulses with period  $T_R$ . For sufficient high pump power, parametric down conversion in the  $\chi^{(2)}$  crystal produces a signal and idler field at frequencies  $\omega_2$  and  $\omega_3$ , respectively. Only the signal is resonated, while the idler is regenerated from noise at each round trip.

presence of noise amplification, the feedback allows the signal to develop in a form that is optimal for energy extraction from the pump. In some respects the output is similar to that of an above-threshold SPOPO. For example, the power spectrum of the noise-driven signal field is double peaked and asymmetric, as is the case for standard SPOPO pulses [22,23]. On the other hand, the signal field reported here is very different from the standard above-threshold SPOPO output; first, should noise be switched off, the signal field would rapidly decay to zero, i.e., to the stable solution; second, if the pump is not saturated, then the amplitude of the signal is proportional to that of the noise or to the noise amplification factor (see Sec. III).

The sensitivity to noise of the SPOPO allows subthreshold operation of the device and opens up the extremely interesting possibility of relating the spectral and correlation properties of the noisy macroscopic pulses to the cavity quantum fluctuations [24,25]. We will study the spectral properties of the signal pulse in the context of quantum optics in another publication. Here we want to address the question of how the noise amplification factor of the SPOPO varies with its parameters. This knowledge may allow in future to tune SPOPOs to the regime that is most of interest to any particular application. Here, we show that the tools of non-normal operators allow us to characterize the SPOPO giant amplification factor as a function of its parameters. Moreover, in doing this we also obtain guidance to the physical origin of this remarkable phenomenon.

The structure of this paper is as follows: in Sec. II we derive the SPOPO model. Section III contains the analysis of giant noise amplification as a function of some of the SPOPO parameters, namely, pump amplitude, the detuning between  $T_R$  and  $T_C$  and, finally, the difference of group velocity between the three fields. The paper is closed by a summary of the main results and a discussion of the issues that are still open. The Appendix contains an overview of non-normal operators and pseudospectra illustrated using a particularly simple example.

## II. SPOPO MODEL

The SPOPO configuration considered in this paper is represented schematically in Fig. 1. It is convenient to write the SPOPO equations in the reference frame of the pump pulse: in this frame we just need to integrate the equations in a small region around the pump pulse because it is not possible for the signal and idler fields to have significant energy away from it. We indicate with  $(z', t')$  the coordinates in the laboratory frame, used in Fig. 1, and with  $z = z'$  and  $t = t' + v_1^{-1}z'$  the coordinates in the pump pulse reference frame. The SPOPO equations in the pump reference frame are

$$\partial_z E_1 = -(\rho_1 - i\Delta k)E_1 + i\beta_1 \partial_t E_1 - E_2 E_3 + \xi_1, \quad (1)$$

$$\partial_z E_2 = -\gamma_2 \partial_t E_2 - \rho_2 E_2 + i\beta_2 \partial_t E_2 + E_1 \bar{E}_3 + \xi_2, \quad (2)$$

$$\partial_z E_3 = -\gamma_3 \partial_t E_3 - \rho_3 E_3 + i\beta_3 \partial_t E_3 + E_1 \bar{E}_2 + \xi_3, \quad (3)$$

where  $E_j$ ,  $j=1,2,3$  are, respectively, the pump, signal and idler slowly varying amplitudes,  $v_j$  their group velocities,  $\beta_j$

TABLE I. Parameter values for the reference noise-sensitive SPOPO configuration. These are the parameters used in the noise-sensitive simulation discussed in Ref. [22] and correspond to those for lithium niobate [21]. One unit of dimensionless time is equivalent to 137 ps and the length of the crystal is 20 mm. The value of the pump amplitude chosen is 87% of threshold, i.e.,  $\rho(\mathcal{L}) \approx 0.87$ .

$\gamma_j = \{0, -0.0166, -0.0049\}$	
$\beta_j = \{-1.29, -0.343, 1.47\} \times 10^{-7}$	
$P_a = 3.6 \Rightarrow \rho(\mathcal{L}) \approx 0.87$	
$\rho_j = \{0, 0, 0\}$	$\Delta k = 0$
$\theta = 0$	$R = 0.14$
$\tau_p = 0.0244$	$\tau_c = -7 \times 10^{-4}$
$A_j = 10^{-8}$	$B_j = 0$

their dispersion coefficients,  $\rho_j$  their losses during propagation and  $\gamma_j = v_j^{-1} - v_1^{-1}$ . The overbar symbol indicates complex conjugate. Time is scaled to the time taken by the pump pulse to traverse the crystal and distances are scaled to the length of the crystal; in these units  $v_1 = 1$ . The field amplitudes are scaled with [21,26]

$$\mu_j = \frac{c}{d_{eff}L} \sqrt{\frac{n_{j+1}n_{j+2}}{\omega_{j+1}\omega_{j+2}}},$$

where  $c$  is the speed of light in vacuum,  $d_{eff}$  is the effective nonlinear coefficient for the three-wave interaction,  $L$  is the crystal length,  $n_j$  is the refractive index of the  $j$ th field,  $\omega_j$  its frequency and the subscripts permute cyclically. Finally, the term  $\xi_j \equiv \xi_j(z, t)$  is a Gaussian noise of amplitude  $A_j$   $\delta$ -correlated in both space and time that represents noise sources inside the crystal.

These equations are complemented by the initial conditions

$$E_1(0, t) = P(t) + \psi_1(t), \quad E_3 = \psi_3(t), \quad (4)$$

$$E_2(0, t) = \exp(-i\theta) \sqrt{R} E_2(1, t + 1 + \gamma_2 - T_c) + \psi_2(t), \quad (5)$$

where  $P(t) = P(t + T_R)$  is the pump profile, assumed to be periodic with period  $T_R$ .  $T_c$  is the signal cavity round trip time,  $R$  is the total intensity reflection coefficient of the cavity,  $\theta$  is the phase shift acquired per pass by the signal field,  $\psi_j(t)$  is a  $\delta$ -correlated Gaussian noise of amplitude  $B_j$  that represents external noise sources on the field  $E_j$ . In all simulations reported here we have assumed that these noise terms have zero amplitude (see Table I). We have, however, verified that all results are independent of whether the noise is injected in the crystal ( $A_j \neq 0$ ) or at the boundary ( $B_j \neq 0$ ). Finally, we assume that the pump profile is a Gaussian

$$P(t) = \begin{cases} P_a \exp(-t^2/\tau_p^2), & -T_R \leq t < T_R, \\ P(t + T_R) = P(t) & \end{cases}$$

of amplitude  $P_a$  and width  $\tau_p \ll T_R$ .

We can recast the SPOPO equations as a stroboscopic map synchronous with the pump pulses, i.e., as a mathematical relation between the signal pulses generated by successive pump pulses. Roughly speaking, since the signal is ap-

proximately synchronous with the pump, we can think of this map as a round trip map that expresses the pulses at one round trip in terms of the fields at the previous one. With this proviso, we normally refer to the  $n$ th iteration of this map as the “ $n$ th round trip.” Formally, we introduce a new time variable,  $\tau$ ,  $-T_R/2 \leq \tau < T_R/2$ , to measure the time elapsed since the center of the  $n$ th pump pulse,  $t(n, \tau) = \tau + nT_R$ ,  $n \in \mathbb{N}$ . We also define the fields at the  $n$ th round trip to be  $E_j^{(n)}(z, \tau) \equiv E_j(z, \tau + nT_R)$ . The equations for the fields  $E_j^{(n)}$  are unchanged from Eqs. (1)–(3) with  $t$  replaced by  $\tau$  and  $E_j$  by  $E_j^{(n)}$ . The boundary conditions are

$$E_1^{(n)}(0, \tau) = P(\tau) + \psi_1(\tau), \quad E_3^{(n)}(0, t) = \psi_3(\tau), \quad (6)$$

$$E_2^{(n)}(0, \tau) = \exp(-i\theta)\sqrt{R}E_2^{(n-1)}(1, \tau + 1 + \gamma_2 + \tau_c) + \psi_2(\tau), \quad (7)$$

where  $\tau_c \equiv T_R - T_c$  is the detuning between pump and signal periods. With a slight abuse of notation we have indicated the noise terms as  $\psi_j(\tau)$ , even though the realization of the noise is different at each round trip. The SPOPO map consists in using Eqs. (1)–(3) to take the fields  $E_j^{(n-1)}(0, t)$  from  $z=0$  to  $z=1$  and then Eqs. (6) and (7) to map the fields from round trip  $n-1$  to round trip  $n$ .

The SPOPO equations without noise ( $A_j=B_j=0$ ) admit a zero-signal and idler solution ( $E_2^{(n)}=E_3^{(n)}=0$ ) with pump field  $E_1^{(n)}(z, \tau)$  given at each round trip by the solution of Eq. (1) with  $E_2^{(n)}=E_3^{(n)}=0$  and with initial condition  $E_1^{(n)}=P(\tau)$ .

The zero-signal and idler solution is stable for sufficiently small pump power, i.e., if  $P_a$  is sufficiently small. To study its stability we need to linearize Eqs. (1)–(3) around it, assuming  $A_j=0$ . They become

$$\partial_z e_1^{(n)} = -(\rho_1 - i\Delta k)e_1^{(n)} + i\beta_1 \partial_{\tau\tau} e_1^{(n)}, \quad (8)$$

$$\partial_z e_2^{(n)} = -\gamma_2^{-1} \partial_{\tau} e_2^{(n)} - \rho_2 e_2^{(n)} + i\beta_2 \partial_{\tau\tau} e_2^{(n)} + E_1^{(n)} e_3^{(n)}, \quad (9)$$

$$\partial_z e_3^{(n)} = -\gamma_3^{-1} \partial_{\tau} e_3^{(n)} - \rho_3 e_3^{(n)} + i\beta_3 \partial_{\tau\tau} e_3^{(n)} + E_1^{(n)} e_2^{(n)}, \quad (10)$$

where  $e_j$ 's are the perturbations of the three fields and  $E_1^{(n)}$  is the zero-signal pump field. These equations are complemented by the boundary conditions (with  $B_j=0$ )

$$e_1^{(n)}(0, \tau) = 0, \quad (11)$$

$$e_2^{(n)}(0, \tau) = \exp(-i\theta)\sqrt{R}e_2^{(n-1)}(1, \tau + \tau_c + 1 + \gamma_2), \quad (12)$$

$$e_3^{(n)}(0, t) = 0. \quad (13)$$

The perturbation of the pump field is decoupled from those of the other fields. Equation (8) with boundary condition (11) has solution  $e_1^{(n)}(z, \tau) \equiv 0$ . All the dynamics is therefore contained in the equations for the perturbations of the signal and idler driven by the unperturbed pump field, Eqs. (9) and (10) with boundary conditions (12) and (13). These can be written formally as a linear operator  $\mathcal{L}$  that maps the perturbation on the signal field from one round trip to the next,

$$e_2^{(n)}(0, \tau) = \mathcal{L}e_2^{(n-1)}(0, \tau). \quad (14)$$

The stability properties and the noise sensitivity of the zero-signal solution are directly related to the spectrum and pseudospectrum of  $\mathcal{L}$ . In particular, the SPOPO is above threshold when the spectral radius,  $\rho(\mathcal{L})$ , of  $\mathcal{L}$ , i.e., the largest of the absolute values of the eigenvalues of  $\mathcal{L}$ , is larger than one. Below threshold, the SPOPO can still amplify random noise to produce macroscopic pulses when the system is strongly non-normal and the boundaries of the pseudospectrum are sufficiently far from the unitary circle corresponding to the threshold.

In the pulsed regime of interest to this paper the nonlinear SPOPO map, Eqs. (1)–(3) and Eqs. (6) and (7), and their linearized version, Eqs. (8)–(10) and Eqs. (11)–(13), are only amenable to a numerical study. We have used a split step method, comprising a Fourier transform in time and second order Runge-Kutta in the longitudinal coordinate, to integrate the nonlinear SPOPO equations in the crystal. A  $\delta$ -correlated Gaussian noise is added after each space step to represent noise in the parametric interaction. After integrating one propagation through the crystal, Eq. (7) is applied to the signal field using a Fourier and anti-Fourier transform pair.

In order to study the stability of the zero-signal and idler solution we need to determine the structure of the spectrum of the linear stability operator  $\mathcal{L}$ . We represent this operator as a matrix on a suitable basis of  $M$  Fourier modes  $\exp(-i\omega_m \tau)$ , with  $\omega_m = m\Delta\omega$ ,  $n = -M/2, \dots, M/2-1$  and  $\Delta\omega$  a suitably chosen discretization parameter. In this way the matrix representation of  $\mathcal{L}$  can be computed efficiently using a standard FFT algorithm. Once this representation has been obtained the spectrum and pseudospectrum are computed using the MATLAB Singular Value Decomposition routine [27].

In all numerical simulations we have checked for convergence by comparison with simulations with either a larger number of Fourier modes and/or smaller discretization step in the longitudinal direction.

### III. PARAMETER DEPENDENCE OF THE TRANSIENT AMPLIFICATION

#### A. Introduction

The SPOPO model considered in this paper was shown in [21] to be noise sensitive. This work was extended in [22] where the pseudospectrum of the linearized map  $\mathcal{L}$ , Eq. (14), was computed. In particular, in this paper it was shown that the Kreiss constant of  $\mathcal{L}$ , which provides a lower bound to the maximum noise amplification, see the Appendix, can be as large as  $10^9$  for experimentally realistic parameter values. Here we want to extend these results and study the SPOPO noise amplification factor as a function of some of its parameters. The SPOPO equations have far too many parameters to allow for a systematic study of the entire parameter space. Here we have chosen to use the noise-sensitive simulation of Ref. [22], parameters in Table I, as a reference configuration and have studied how the noise amplification factor changes as some of the parameters are varied with respect to this configuration. We have chosen two parameters, the pump

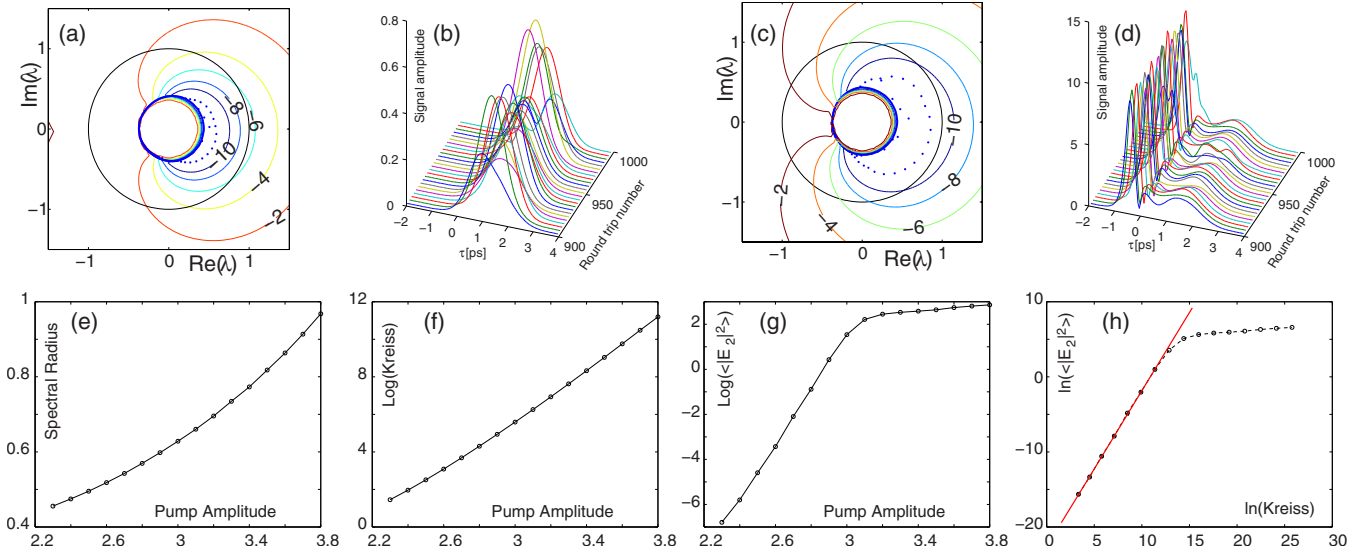


FIG. 2. (Color online) Pseudospectrum, (a) and (c), and signal intensity as a function of time and round trip, (b) and (d), for  $P_a = 2.9$  and  $P_a = 3.6$ , (a) and (b) and (c) and (d), respectively. In all pseudospectra plots the dots are the eigenvalues of  $\mathcal{L}$  and the contour lines correspond to constant values of  $\log_{10}(\|(z - \mathcal{L})^{-1}\|)$ , see Eq. (A4). (e) Spectral radius, (f) Kreiss constant, and (g) average signal energy as a function of the pump amplitude  $P_a$ . (h) Log-log plot of the average signal energy as a function of the Kreiss constant. The straight solid line represents a best fit of the corresponding data points (slope 2.1). All parameters except  $P_a$  as in Table I.

amplitude  $P_a$  and the detuning  $\tau_c$ , because they are of easy experimental access. We have also studied the effect of the group velocity to gain a better qualitative understanding of the physical mechanism of giant noise amplification.

### B. Effect of the pump amplitude

We have varied the pump parameter of the reference configuration in the range  $2.3 \leq P_a \leq 3.8$ . The pump value affects directly the spectral radius  $\rho(\mathcal{L})$  and the Kreiss constant  $\mathcal{K}$ , which increase from 0.45 to 0.97 and 28 to  $1.5 \times 10^{11}$ , respectively. Their graphs are shown in Figs. 2(e) and 2(f). The spectrum and pseudospectrum for the reference configuration,  $P_a = 3.6$ , and for a lower power,  $P_a = 2.9$ , are shown in Figs. 2(c) and 2(a) respectively. From these graphs we can see that the spectral properties of  $\mathcal{L}$  do not change significantly with the pump power. The signal amplitude at corresponding powers, also shown in Fig. 2, indicate that the pulse become narrower and more intense as the system gets closer to threshold. These features are also preserved when passing the threshold: the over-threshold pulse is narrow and noise dominated, just as the signal below threshold. The average signal energy increases with the pump power, until saturation sets in, see Fig. 2(g). In the nonsaturated regime it is proportional to  $\mathcal{K}^2$ , see Fig. 2(h): a best fit of the log-log plot of the average signal energy versus the Kreiss constant gives a slope of 2.1. This result is in good agreement with the analysis of the response [Eq. (A7)] of the simple system [Eq. (A6)] to a stochastic modulation. The counterpart of this phenomenon is that the amplitude of the signal in the nonsaturated regime is directly proportional to the amplitude of the noise (see Table II). This is in stark contrast to the above-threshold behavior of a laser, for example, where the amplitude of the output field is proportional to the distance of the

pump from threshold and independent of the amplitude of the noise fluctuations.

### C. Effect of the pump-signal period detuning

The intuitive, if simplistic, physical explanation of giant noise amplification is that the signal pulse arrives at the crystal later than the pump pulse. Hence the noisy leading edge of the signal is amplified, while the trailing edge is damped by the cavity losses. We expect, therefore, that sensitivity to noise, parametrized by the Kreiss constant, will decrease as  $\tau_c$  becomes positive. This is indeed the case: for  $\tau_c = 3.5 \times 10^{-4}$  there is no macroscopic subthreshold signal field. This appears for  $\tau_c = 1.75 \times 10^{-4}$ , but has a very regular appearance, see Fig. 3(b), even though the Kreiss constant for this configuration is quite large,  $\mathcal{K} \approx 10^9$ . The spectrum and

TABLE II. Peak amplitude of the signal averaged over 900 round trips and corresponding amplitude of the noise. In the case of the middle column,  $P_a = 3.0$ : the SPOPO is far from saturation and the two amplitudes are approximately linearly proportional. The first value is lower than expected because of saturation of the pump pulse, while the last is larger because the noise of numerical computations is comparable to the noise added in this simulation. In the case of the right column,  $P_a = 3.6$ , the SPOPO is in the pump saturation regime and the two amplitudes are not linearly proportional. All other parameters as in Table I.

Noise amplitude	$\langle \max  E_2  \rangle \times 10^{-3}$	$\langle \max  E_2  \rangle$
$10^{-9}$	155	8.58
$10^{-10}$	16.3	7.30
$10^{-11}$	1.62	5.26
$10^{-12}$	0.168	2.11

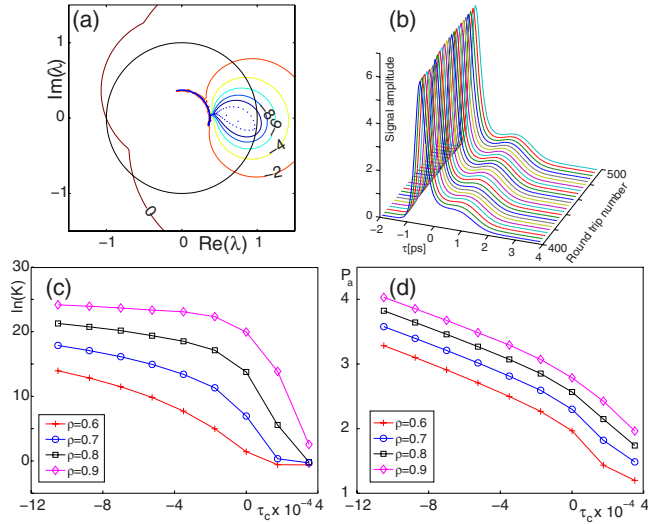


FIG. 3. (Color online) (a) Pseudospectra and signal amplitude as a function of time and round trip number (b) for  $\tau_c = 1.75 \times 10^{-4}$  and  $P_a = 2.6$  (equivalent to 98% of threshold). (c) Plot of  $\ln(K)$  as a function of  $\tau_c$  for different values of the spectral radius,  $\rho(\mathcal{L})$ . (d) Pump amplitude  $P_a$  at constant spectral radius as a function of  $\tau_c$ . All other parameters as in Table I.

pseudospectrum for these parameter values, Fig. 3(a), are very different from those in the reference configuration, Fig. 2(c). It is only for negative values of  $\tau_c$  that the system displays the features of the reference configuration. The main points to notice are that (1)  $K$  at constant  $\rho(\mathcal{L})$  decreases with increasing  $\tau_c$ , see Fig. 3(c); (2) there is a maximum value of  $\tau_c$  for a given value of  $K$ , see Fig. 3(c); (3) the pump power needed to obtain a given  $\rho(\mathcal{L})$  increases with decreasing  $\tau_c$ , see Fig. 3(d).

#### D. Effect of the group velocity difference

Finally, we have studied the effect of the group velocity on giant noise amplification to see what role this parameter plays in the intuitive  $\tau_c$ -dominated explanation of this phenomenon given at the beginning of Sec. III C. To study the effect of the group velocity difference we have scaled the reference group velocities  $\gamma_j$  listed in Table I by a scaling factor  $\gamma_s$ . In particular,  $\gamma_s = 0$  corresponds to a SPOPO where

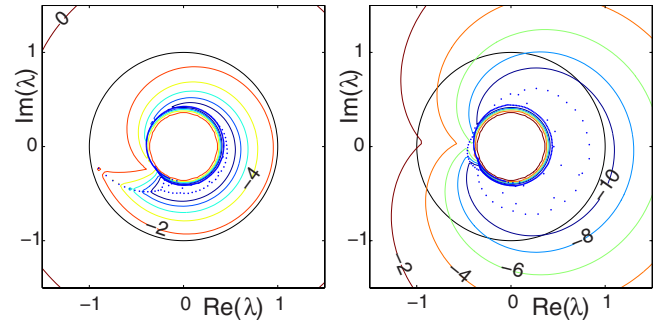


FIG. 4. (Color online) Pseudospectra for  $\gamma_s = 0.2$  (left) and  $\gamma_s = 0.6$  (right). The pump amplitudes are  $P_a = \{1.8, 3.2\}$ , respectively, corresponding to 93% and 84% of threshold. All other parameters as in Table I.

all fields travel with the same group velocity, while  $\gamma_s = 1$  is the reference configuration.

For  $\gamma_s < 0.4$  the bifurcation from the zero field solution is completely different from the reference configuration. The loss of stability is through an eigenvalue with negative real part crossing the unit circle (see left panel of Fig. 4). The pseudospectrum is very close to the spectrum and the SPOPO is not noise sensitive: there is no macroscopic signal below threshold and above threshold the signal pulse is time stationary and of width similar to that of the pump pulse. For  $\gamma_s \geq 0.4$ , instead, the behavior of the SPOPO is very similar to that of the reference configuration: the zero field solution loses stability because an eigenvalue with positive real part crosses the unit circle; the pseudospectrum extends well beyond the unit circle and the SPOPO is noise sensitive. A typical pseudospectrum, with  $\gamma_s = 0.8$  is shown on the right hand panel of Fig. 4. The main conclusions that can be drawn from the analysis for  $0.4 \leq \gamma_s \leq 1.6$  are (1) the pump power needed to obtain a given  $\rho(\mathcal{L})$  grows with  $\gamma_s$ , see Fig. 5(a); (2) the pump power required to obtain a given value of the Kreiss constant increases with  $\gamma_s$ , see Fig. 5(b); (3) the average intensity of the signal pulse is proportional to  $K^2$ , until saturation sets in, see Fig. 5(c) where the best fit line has slope two. This is in accordance to the response to noise of the simple model analyzed in the Appendix, Eq. (A7); (4) the maximum value of the Kreiss constant is not strongly dependent of  $\gamma_s$ , see Fig. 5(d), for  $\gamma_s$  above the threshold value for noise sensitivity.

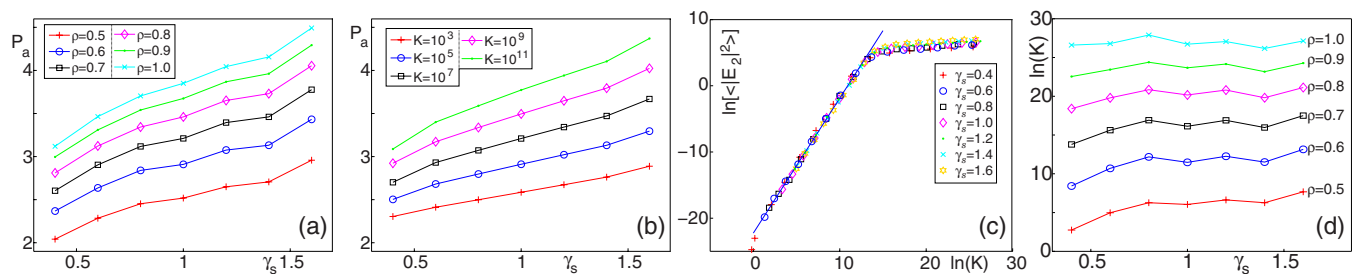


FIG. 5. (Color online) (a) Pump amplitude  $P_a$  as a function of  $\gamma_s$  for different values of the spectral radius  $\rho(\mathcal{L})$ . (b) Pump amplitude  $P_a$  as a function of  $\gamma_s$  for different values of the Kreiss constant  $K$ . (c) Log-log plot of the average signal field intensity as a function of the Kreiss constant  $K$ . The different symbols correspond to different values of  $\gamma_s$  in the range  $[0.4, 1.6]$ . (d) Kreiss constant as a function of  $\gamma_s$  for different values of the spectral radius  $\rho(\mathcal{L})$ .

#### IV. CONCLUSIONS

The analysis of the SPOPO parameters detailed in Sec. III shows that giant amplification depends on the group velocity and not just on the pump-signal detuning  $\tau_c$ , even though this parameter certainly plays a key role. In particular, for low values of the group velocity there is no significant noise amplification. However, once a threshold value for the group velocity difference has been reached, then the noise amplification factor is more or less independent of the group velocity and increases with the pump amplitude or the magnitude of the pump-signal detuning. In Sec. III we have varied only three of the SPOPO parameters. It is, however, possible to study in detail the SPOPO behavior in any parameter region that may be of interest.

This opens the possibility of tailoring the SPOPO parameters to specific applications, either to minimize or to maximize noise sensitivity. The possibility of using the giant amplification rates that the SPOPO is capable of is especially enticing. First of all, it should be possible to seed the SPOPO with a small modulation and obtain a controllable, high-intensity signal in the region where the device would be noise dominated, similar to what was proposed in [21]. This might be useful to obtain reproducible signal pulses in experiments where the control parameters are limited to the noise-sensitive region. Second, the quantum properties of SPOPOs have long been a subject of study [28,29] and there has been considerable debate in the literature on whether it would be possible to use pattern formation in optical parametric oscillators to detect cavity quantum fluctuations [30–33]. The giant noise amplification measured and characterized in this paper leads to a definite possibility of detecting the noise quantum signature in the macroscopic sub-threshold signal and idler fields emitted by the SPOPO. We are currently developing a quantum optics model of SPOPO that can be used to answer this question.

#### ACKNOWLEDGMENT

We wish to thank Gian-Luca Oppo for his help and support.

#### APPENDIX: NON-NORMAL OPERATORS

##### 1. Simple example

It is well known that the fixed points of a (hyperbolic) dynamical systems are stable if all eigenvalues of the equations linearized around the fixed point have negative real part [34]. Stability, in this sense, means that in the *absence* of noise, any sufficiently small initial perturbation decays *asymptotically* to zero. There is nothing in this definition that stops an initial perturbation from growing before reaching the asymptotic regime of decay. This phenomenon is called transient growth. The presence of noise adds another facet to the issue of stability: if noise is present, the system is never able to return and settle at the stable equilibrium. Noise induced fluctuations will continually force it to move around the equilibrium point. In a system with large transient growth the noise fluctuations may well not be small, even though

they will always ultimately proportional to the noise amplitude.

Transient growth is a phenomenon characteristic of systems whose linearized equations have non-normal coefficient matrix, i.e., a matrix that does commute with its adjoint [7,8,10]. Geometrically, these matrices are characterized by having nonorthogonal eigenvectors. Here we illustrate these phenomena with a simple example that contains, in a very simplified manner, the main features of the SPOPO equations.

Consider the system of two linear differential equations

$$\dot{\mathbf{x}} = M_2 \mathbf{x}, \quad M_2 = \begin{pmatrix} -1 & 9 \tan(\theta) \\ 0 & -10 \end{pmatrix}. \quad (\text{A1})$$

This has a stable fixed point at  $\mathbf{x}=(0,0)$  with eigenvalues and eigenvectors

$$\lambda_1 = -1, \quad \mathbf{v}_1 = (1,0); \quad \lambda_2 = -10, \quad \mathbf{v}_2 = (-\sin \theta, \cos \theta).$$

For  $\theta=0$  the matrix  $M_2$  is normal and the eigenvalues are orthogonal. For  $\theta \neq 0$  the matrix  $M_2$  is non-normal and its eigenvectors are no longer orthogonal, but form an angle equal to  $\pi/2 + \theta$ . As  $\theta$  tends to  $\pi/2$  the eigenvectors become closer and closer to being parallel. An initial condition that is the (small) difference of two very large eigenvectors will grow considerably before eventually decreasing. To quantify the transient growth of Eq. (A1), we start by noting that its solution with initial condition  $\mathbf{x}_0$  is  $\mathbf{x}(t) = \exp(tM_2)\mathbf{x}_0$ . Hence, the maximum growth at any given time  $t$  of the solution  $\mathbf{x}(t)$  is

$$\sup_{\mathbf{x}_0} \frac{\|\mathbf{x}(t)\|}{\|\mathbf{x}_0\|} = \|\exp(tM_2)\|.$$

For  $\theta \leq \pi/2$  (and using the two-norm) the maximum transient growth is

$$\sup_{t>0} \|\exp(tM_2)\|_2 \approx 0.7 \tan(\theta). \quad (\text{A2})$$

In other words, the system (A1) can display transient growth as large as one wishes, provided that  $\theta$  is sufficiently close to  $\pi/2$ .

##### 2. Pseudospectra

Equation (A1) is simple enough that it is possible to compute analytically the transient amplification factor of a perturbation of the initial condition. It is important, however, to develop tools that allow to determine the response of more complicated systems to generic perturbations, e.g., a forcing term. In particular, from the point of view of applications, it is especially important to know the frequency dependence of the amplification factor of a periodic forcing term. The key to answering these questions is the resolvent of the coefficient matrix of the model equations linearized around the fixed point. The asymptotic amplitude  $\mathbf{x}_\infty$  of the response of a linear system

$$\dot{\mathbf{x}} = M\mathbf{x} + \mathbf{f}(t) \quad (\text{A3})$$

to a modulation  $\mathbf{f}(t) = \mathbf{f}_0 e^{z t}$ ,  $z \in \mathbb{C}$ , is given by

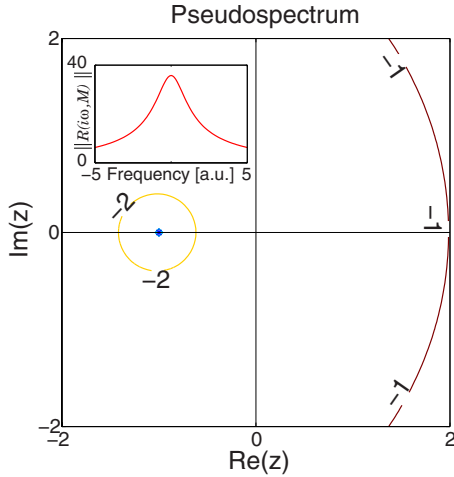


FIG. 6. (Color online) Pseudospectrum and frequency response (inset) of system [Eq. (A1)] for  $\theta=1.568$ . The dot corresponds to the eigenvalue  $\lambda=-1$ . The contour lines correspond to constant values of  $\log_{10}(\|R(z, M)\|)$ , see Eq. (A4).

$$\mathbf{x}_\infty = (z - M)^{-1} \mathbf{f}_0,$$

provided that all the eigenvalues of  $M$  have negative real part. The amplification factor is

$$\sup_{\mathbf{f}_0} \frac{\|\mathbf{x}_\infty\|}{\|\mathbf{f}_0\|} = \|(z - M)^{-1}\| \equiv \|R(z, M)\|,$$

where  $R(z, M)$  is the resolvent of  $M$ . This last equation tells us that the norm of the resolvent is the amplification factor of an exponential perturbation with complex exponent  $z$ . Therefore, the graph of the norm of the resolvent in the complex plane gives a pictorial representation of the amplification factor. This idea is formalized by the definition of  $\epsilon$ -pseudospectrum (or pseudospectrum) [9]. For every  $\epsilon > 0$  we define the  $\epsilon$ -pseudospectrum as the set

$$\Lambda_\epsilon(M) = \{z \in \mathbb{C} \mid \|R(z, M)\| \geq \epsilon^{-1}\}, \quad \epsilon > 0. \quad (\text{A4})$$

The  $\epsilon$ -pseudospectra form a nested set. They tend to the spectrum of  $M$  as  $\epsilon \rightarrow 0$  and to the complex plane as  $\epsilon \rightarrow \infty$ . Very roughly, the pseudospectrum is the set of contour levels of  $\|R(z, M)\|$ . If the exponent (frequency) of the modulation is within the contour level corresponding to  $\epsilon$  then we can expect that the system will amplify the modulation by a factor approximately equal to  $1/\epsilon$ . In particular, the intersection of the imaginary axis with the pseudospectrum gives the transient amplification factor of the system to a periodic modulation of frequency  $\omega$ , with  $z=i\omega$ . The pseudospectrum of Eq. (A1) is plotted in Fig. 6. The inset of this figure shows the cross-section of the pseudospectrum with the imaginary axis: this is the frequency response of the system to a periodic modulation.

The pseudospectrum is also related to the magnitude of the transient growth,  $\sup_{t>0} \|\exp(tM)\|$ . It can be shown that [8]

$$\sup_{t>0} \|\exp(tM)\| \geq \mathcal{K}(M),$$

where the constant  $\mathcal{K}$ , called the Kreiss constant of the matrix  $M$ , is defined as

$$\mathcal{K}(M) \equiv \sup_{\epsilon>0} \frac{\alpha_\epsilon(M)}{\epsilon} = \sup_{\Re(z)>0} \Re(z) \|R(z, M)\|. \quad (\text{A5})$$

Here  $\alpha_\epsilon(M)$  is the  $\epsilon$ -pseudospectral abscissa of the  $\epsilon$ -pseudospectrum of  $M$ , i.e., the largest real part of all the elements of the set  $\Lambda_\epsilon(M)$ . For the system (A1) the value of the Kreiss constant using the two-norm is approximately  $\mathcal{K}(M) \approx 0.5 \tan(\theta)$ , which is a good estimate of the maximum transient growth, Eq. (A2).

Finally, we consider the effect of adding a Gaussian  $\delta$ -correlated noise to Eq. (A1),

$$\dot{\mathbf{x}} = M\mathbf{x} + \sigma \mathbf{f}(t), \quad \langle f_i(t) f_j(t') \rangle = \delta_{ij} \delta(t - t'). \quad (\text{A6})$$

This equation can be written as an Ornstein-Uhlenbeck equation for the vectorial stochastic variable  $\mathbf{x}(t)$  which can be solved by standard stochastic calculus techniques [35]. The asymptotic value of the average is zero, while that of the variance for  $\theta$  close to  $\pi/2$  is

$$\langle \|\mathbf{x}(t)\|^2 \rangle \simeq 30\sigma^2 \tan^2(\theta), \quad \theta \lesssim \pi/2. \quad (\text{A7})$$

This results shows that the average ‘‘intensity’’ of the signal is proportional to  $\mathcal{K}^2$ , a result that also holds for the SPOPO equations.

### 3. Non-normal maps

The results and concepts introduced in the previous section carry more or less unchanged to maps, i.e., relations that express the state of the system at stage  $n+1$ ,  $\mathbf{x}^{(n+1)}$ , in terms of its previous state as

$$\mathbf{x}^{(n+1)} = M\mathbf{x}^{(n)}, \quad (\text{A8})$$

with  $M$  an  $m \times m$  matrix, possibly obtained by linearizing a nonlinear map around one of its fixed point. If the matrix  $M$  is non-normal the system (A8) may display transient growth. The definition (A4) of pseudospectrum remains unchanged, while the Kreiss constant for maps is defined as [8]

$$\mathcal{K} = \sup_{\epsilon>0} \mathcal{K}_\epsilon, \quad \text{with} \quad \mathcal{K}_\epsilon \equiv \frac{\rho_\epsilon(\mathcal{L}) - 1}{\epsilon}, \quad (\text{A9})$$

where  $\rho_\epsilon(\mathcal{L})$  is the radius of the smallest circle in the complex plane that contains  $\Lambda_\epsilon(\mathcal{L})$ . Geometrically,  $\mathcal{K}_\epsilon$  is the maximum distance of the boundary of  $\Lambda_\epsilon(\mathcal{L})$  from the unitary circle divided by  $\epsilon$ . The Kreiss constant is still a lower bound for the maximum transient growth, now given by  $\max_n \|M^n\|$ .

- [1] R. Benzi, A. Sutera, and A. Vulpiani, *J. Phys. A* **14**, L453 (1981).
- [2] K. Petermann, *IEEE J. Quantum Electron.* **15**, 566 (1979).
- [3] W. J. Firth and A. M. Yao, *Phys. Rev. Lett.* **95**, 073903 (2005).
- [4] S. Longhi and P. Laporta, *Phys. Rev. E* **61**, R989 (2000).
- [5] J. B. Geddes, W. J. Firth, and K. Black, *SIAM J. Appl. Dyn. Syst.* **2**, 647 (2003).
- [6] F. Papoff, G. D'Alessandro, and G.-L. Oppo, *Phys. Rev. Lett.* **100**, 123905 (2008).
- [7] L. N. Trefethen, A. E. Trefethen, S. C. Reddy, and T. A. Driscoll, *Science* **261**, 578 (1993).
- [8] L. N. Trefethen and M. Embree, *Spectra and Pseudospectra* (Princeton University Press, Princeton, NJ, 2005).
- [9] L. N. Trefethen, *SIAM Rev.* **39**, 383 (1997).
- [10] M. Embree and L. N. Trefethen, *The Pseudospectra Gateway*, <http://web.comlab.ox.ac.uk/pseudospectra/>
- [11] G. Szirmai, D. Nagy, and P. Domokos, *Phys. Rev. Lett.* **102**, 080401 (2009).
- [12] M. Sempf, P. Merkel, E. Strumberger, C. Tichmann, and S. Gunter, *New J. Phys.* **11**, 053015 (2009).
- [13] B. F. Farrell and P. J. Ioannou, *J. Atmos. Sci.* **53**, 2025 (1996).
- [14] B. Farrell and P. Ioannou, *J. Atmos. Sci.* **53**, 2041 (1996).
- [15] P. J. Schmid, *Annu. Rev. Fluid Mech.* **39**, 129 (2007).
- [16] J. D. V. Khaydarov, J. H. Andrews, and K. D. Singer, *J. Opt. Soc. Am. B* **12**, 2199 (1995).
- [17] L. Lefort, K. Puech, S. D. Butterworth, Y. P. Svirko, and D. C. Hanna, *Opt. Lett.* **24**, 28 (1999).
- [18] M. V. O'Connor, M. A. Watson, D. P. Shepherd, D. C. Hanna, J. H. V. Price, A. Malinowski, J. Nilsson, N. G. R. Broderick, D. J. Richardson, and L. Lefort, *Opt. Lett.* **27**, 1052 (2002).
- [19] J. Prawiharjo, H. S. S. Hung, D. C. Hanna, and D. P. Shepherd, *J. Opt. Soc. Am. B* **24**, 2484 (2007).
- [20] H. S. S. Hung, J. Prawiharjo, N. K. Daga, D. C. Hanna, and D. P. Shepherd, *J. Opt. Soc. Am. B* **24**, 2998 (2007).
- [21] A. J. Scroggie, G.-L. Oppo, and G. D'Alessandro, *J. Opt. Soc. Am. B* **17**, 84 (2000).
- [22] G. D'Alessandro and C. B. Laforet, *Opt. Lett.* **34**, 614 (2009).
- [23] A. Haché, G. R. Allan, and H. M. van Driel, *J. Opt. Soc. Am. B* **12**, 2209 (1995).
- [24] R. Zambrini, S. M. Barnett, P. Colet, and M. San Miguel, *Phys. Rev. A* **65**, 023813 (2002).
- [25] R. Zambrini, S. Barnett, P. Colet, and M. San Miguel, *Eur. Phys. J. D* **22**, 461 (2003).
- [26] O. Svelto, *Principles of Lasers*, 4th ed. (Plenum, New York, 1998).
- [27] L. N. Trefethen, *Acta Numerica* **8** 247 (1999).
- [28] S. Reynaud, C. Fabre, and E. Giacobino, *J. Opt. Soc. Am. B* **4**, 1520 (1987).
- [29] C. Fabre, E. Giacobino, A. Heidmann, and S. Reynaud, *J. Phys. (France)* **50**, 1209 (1989).
- [30] A. Gatti and L. Lugiato, *Phys. Rev. A* **52**, 1675 (1995).
- [31] I. Marzoli, A. Gatti, and L. A. Lugiato, *Phys. Rev. Lett.* **78**, 2092 (1997).
- [32] L. A. Lugiato, A. Gatti, H. Ritsch, I. Marzoli, and G.-L. Oppo, *J. Mod. Opt.* **44**, 1899 (1997).
- [33] C. Szewaj, G.-L. Oppo, A. Gatti, and L. Lugiato, *Eur. Phys. J. D* **10**, 433 (2000).
- [34] P. Glendinning, *Stability, Instability and Chaos: An Introduction to the Theory of Nonlinear Differential Equations* (Cambridge University Press, Cambridge, England, 1994).
- [35] B. Øksendal, *Stochastic Differential Equations: An Introduction with Applications*, 6th ed. (Springer-Verlag, Berlin, 2003).